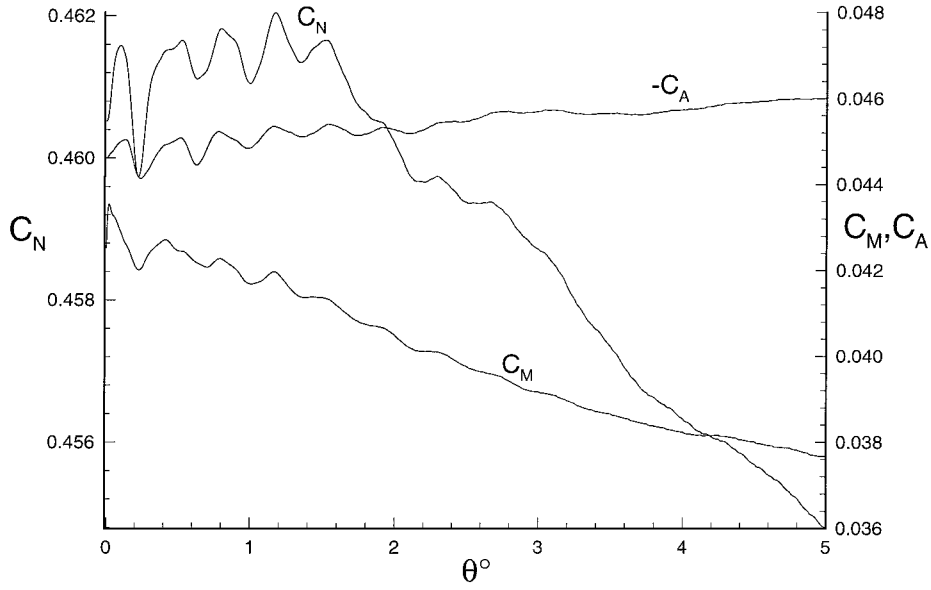

Fig. 5 Histories of force and moment coefficients on hypersonic plane during staging at Mach 5 flight. Pitching center at area centroid: $X_C = -0.466$ and $Y_C = 0.089$.

was available. Hence, the present proof-of-concept simulation was based on the two-dimensional Euler equations solved for an approximate geometry. A more realistic modeling would require the three-dimensional computations including the diffusion terms for the exact geometry. This is currently being pursued.

References

[1]Sakell, L., and Knight, D. D. (eds.), *Proceedings of the First AFOSR Conference on Dynamic Motion Computational Fluid Dynamics*, Rutgers Univ., New Brunswick, NJ, 1996.

[2]Baysal, O., Singh, K. P., and Yen, G.-W., "Dynamic CFD Methods for Prescribed and Aerodynamically-Determined Relative-Moving Multibody Problems," *Proceedings of the First AFOSR Conference on Dynamic Motion CFD*, edited by L. Sakell and D. Knight, Rutgers Univ., New Brunswick, NJ, 1996, pp. 31–44.

[3]Singh, K. P., and Baysal, O., "3D Unstructured Method for Flows Past Bodies in 6-DOF Relative Motion," *Proceedings of 6th International Symposium on CFD*, edited by M. Hafez, Vol. 3, Univ. of California, Davis, CA, 1995, pp. 1161–1168.

[4]Singh, K. P., Newman, J. C., III, and Baysal, O., "Dynamic Unstructured Method for Flows Past Multiple Objects in Relative Motion," *AIAA Journal*, Vol. 33, No. 4, 1995, pp. 641–659.

[5]Rausch, V. L., McClinton, C. R., and Hicks, J. W., "Scramjets Breathe New Life into Hypersonics," *Aerospace America*, Vol. 35, No. 7, 1997, pp. 40–46.

[6]Batina, J. T., "Unsteady Euler Airfoil Solutions Using Unstructured Dynamic Meshes," AIAA Paper 89-0115, Jan. 1989.

[7]Baysal, O., "Flow Analysis and Design Optimization Methods for Nozzle-Afterbody of a Hypersonic Vehicle," *Computational Methods in Hypersonic Aerodynamics*, Kluwer, Dordrecht, The Netherlands, 1992, pp. 341–386.

[8]Baysal, O., and Luo, X.-B., "Computational Aeromechanics Method with Multigrid Accelerated Dual Time Stepping on Unstructured Meshes," *Proceedings of American Society of Mechanical Engineers Fluids Engineering Division Summer Meeting*, American Society of Mechanical Engineers, New York, FEDSM-98-4939, 1998.

[9]Baysal, O., and Luo, X.-B., "Staging of a Hypersonic Vehicle: Numerical Simulations Using Dynamic Unstructured Meshes," *Proceedings of 16th AIAA Applied Aerodynamics Conference*, Reston, VA, 1998, pp. 85–95.

[10]Pirzadeh, S., "Recent Progress in Unstructured Grid Generation," AIAA Paper 92-0445, Jan. 1992.

[11]Hänel, D., Schwane, R., and Seider, G., "On the Accuracy of Upwind Schemes for the Solution of the Navier–Stokes Equations," AIAA Paper 87-1005, Jan. 1987.

[12]Landon, R., "NACA 0012 Oscillatory and Transient Pitching," *Compendium of Unsteady Aerodynamic Measurements*, AGARD Rept. 702, 1982, pp. 3.3–3.25.

V-Tail Stalling at Combined Angles of Attack and Sideslip

Malcolm J. Abzug*
Pacific Palisades, California 90272

Introduction

POSSIBLE stalling of V-tail panels at large combined angles of attack and sideslip has been a concern in flight operations. V-tail panel angles of attack developed by Purser and Campbell[1] apply only to small angles of attack and sideslip. Small-angle results are useful for tail sizing and the calculation of stability derivatives, but this Note extends the Purser and Campbell work to large angles to support studies of possible panel stalling.

Panel Angle-of-Attack Derivation

The geometric angle of attack of a V-tail panel is the angle the local wind makes with a tail chord line, measured in the plane of the airfoil. Neglecting angular velocity, the geometric angles of attack and sideslip of a single V-tail panel are a function only of the following six variables: α and β, the aircraft angles of attack and sideslip; ε and σ, the average downwash and sidewash angles at the V-tail; Γ, the dihedral angle of a V-tail panel, positive for the left panel; and δ, the V-tail incidence or control angle for an all-moving V-tail.

The panel geometric angles of attack and sideslip are found by the matrix operations[2] of Eqs. (1–3). Panel body axes are fixed in the panel with X forward in the chord plane, Z normal to the chord plane pointing down, and Y pointing to the right. Equation (1) represents successive rotations of panel body axes away from aircraft wind axes. In the wind axes used here the X axis points into the relative wind, and X–Z is an aircraft plane of symmetry.

The first two rotations carry aircraft body axes away from wind axes by $\beta + \sigma$ and then $\alpha - \varepsilon$. The third and fourth rotations Γ and then δ establish panel body axes. Tail panel angles of attack and sideslip are found from the wind vector components in the final, rotated position of panel axes. The incidence or control angle δ

Received 27 July 1998; revision received 20 March 1999; accepted for publication 20 March 1999.

*Aeronautical Consultant, 14951 Camarosa Drive. Fellow AIAA.

adds linearly to the panel angle of attack and that rotation need not be made in matrix form.

$$\{\text{pan}\} = [\delta][\Gamma][\alpha - \varepsilon][\beta + \sigma]\{\text{vel}\} \quad (1)$$

$$\alpha_p = \tan^{-1}[\text{pan}(3)/\text{pan}(1)] + \delta \quad (2)$$

$$\beta_p = \sin^{-1}[\text{pan}(2)] \quad (3)$$

In the following expanded forms of the matrices, the symbols s and c representing the sine and cosine functions, respectively. The MATLAB® shorthand matrix notation is used:

{pan} = column matrix of normalized wind vector components on panel body axes, $[\text{pan}(1)\ \ \text{pan}(2)\ \ \text{pan}(3)]^T$
{vel} = column matrix of wind vector components on wind axes, $[1\ \ 0\ \ 0]^T$
$[\beta + \sigma]$ = sideslip + sidewash matrix $[c(\beta+\sigma)\ \ -s(\beta+\sigma)\ \ 0;\ s(\beta+\sigma)\ \ c(\beta+\sigma)\ \ 0;\ 0\ \ 0\ \ 1]$
$[\alpha]$ = angle of attack—downwash matrix $[c(\alpha-\varepsilon)\ \ 0\ \ -s(\alpha-\varepsilon);\ \ 0\ \ 1\ \ 0;\ s(\alpha-\varepsilon)\ \ 0\ \ c(\alpha-\varepsilon)]$
$[\Gamma]$ = dihedral matrix $[1\ \ 0\ \ 0;\ 0\ \ c\Gamma\ \ s\Gamma;\ 0\ \ -s\Gamma\ \ c\Gamma]$
$[\delta]$ = incidence matrix $[c\delta\ \ 0\ \ -s\delta;\ 0\ \ 1\ \ 0;\ s\delta\ \ 0\ \ c\delta]$
α_p = geometric panel angle of attack
β_p = geometric panel sideslip angle, or crossflow

Carrying out the indicated multiplications and other operations of Eqs. (1–3) leads to the V-tail panel angle of attack and sideslip equations:

$$\alpha_p = \tan^{-1}\{[-s\Gamma s(\beta+\sigma) + c\Gamma s(\alpha-\varepsilon)c(\beta+\sigma)]/[c(\alpha-\varepsilon)c(\beta+\sigma)]\} + \delta \quad (4)$$

$$\beta_p = \sin^{-1}[c(\Gamma)s(\beta+\sigma) + s(\Gamma)s(\alpha-\varepsilon)c(\beta+\varepsilon)] \quad (5)$$

Numerical Results

For example calculations, downwash and sidewash variations with angle of attack are chosen that are representative of half-span flaps fully deflected on a low wing airplane, as follows:

$$\varepsilon = \varepsilon_0 + \frac{\partial\varepsilon}{\partial\alpha}\alpha = 4.0 + 0.5\alpha, \qquad \sigma = \frac{\partial\sigma}{\partial\beta}\beta = 0.2\beta \quad (6)$$

Figure 1 maps the panel angles of attack for a 30-deg left V-tail panel (or a right panel of an inverted V-tail) as functions of vehicle angle of attack and sideslip. Tail incidence is zero. To obtain results for a right-hand panel, reverse the signs of the sideslip angles.

Discussion

Assume that an airplane with a 30-deg V-tail is in a landing approach at an angle of attack of 5 deg, giving a trimmed lift coefficient of about 1.1, with flaps down. With the airplane at zero sideslip, the tail panel angle of attack is a moderate −2 deg, well out of the stalled range.

Transient values of sideslip would occur if the approach is made in rough air. The left panel is assumed to stall negatively at a panel angle of attack of −12 deg. This stalled panel angle is reached with a right sideslip angle of 17 deg. With flaps down and at a forward c.g., the net trimming tail load would be down, and stalling of the left panel when right sideslip exceeds 17 deg in a transient yawing motion would cause the airplane to pitch in a nose-down direction. An appreciable panel crossflow value of 17 deg is calculated [Eq. (5)] at the stall point, reached with a right sideslip of 17 deg.

Induction and Crossflow Effects

The antisymmetric additional span load of a V-tail in sideslip acts to reduce panel local angles of attack below those for the same angle of attack, with no sideslip (Fig. 2 in Ref. 1). This effect occurs with any wing in sideslip, which means that slightly higher panel angles of attack can be reached before stall with a V-tail in sideslip, as compared with the same tail without sideslip. Panel crossflow on a V-tail in sideslip operates in the other direction. As in a swept back wing, crossflow lengthens boundary layer runs, leading to earlier separation starting at the trailing edge. This would reduce panel angles of attack for stall on a V-tail in sideslip, as compared with the same tail without sideslip.

Effects of Sidewash and Downwash

Sidewash at a V-tail for an airplane in sideslip is caused mainly by the effect of the fuselage crossflow on the wing spanwise lift distribution. Deflected flaps complicate the problem. Low wing arrangements lead to stabilizing sidewash, such as the 20% figure used in the sample calculations. The calculations for Fig. 1 were repeated for a larger sidewash angle, or $\sigma = 0.5\beta$. That change reduces the sideslip angle for left-panel stall (assumed to occur at a panel angle of attack of −12 deg) by 3 deg, from 17 to 14 deg.

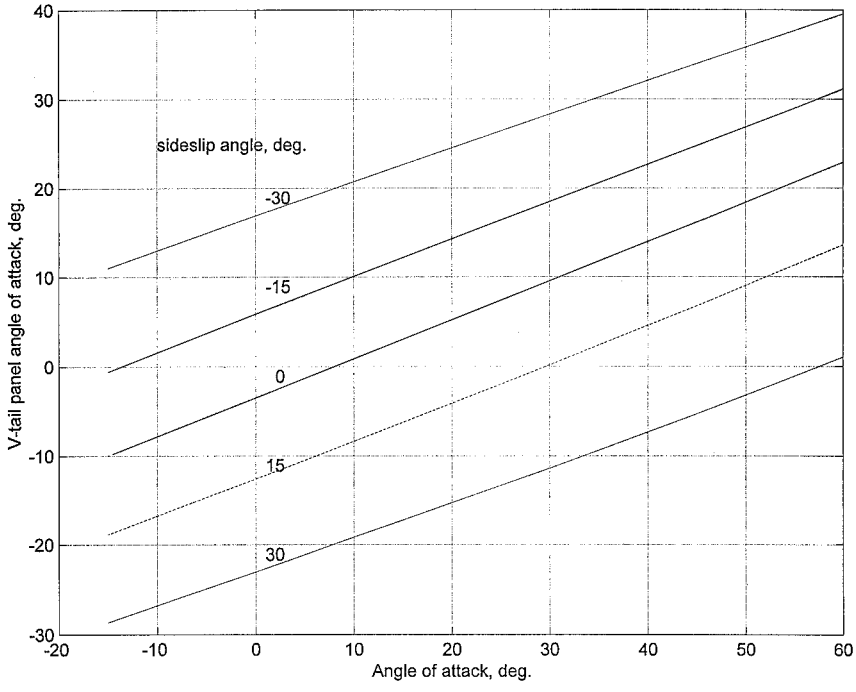

Fig. 1 Geometric panel angles of attack for a V-tail with 30 deg of dihedral. The data incorporate downwash and sidewash values typical of a low-wing airplane with flaps down.

The sideslip angle for left-panel stall is reduced to 12 deg by assuming a larger downwash angle than in the calculations for Fig. 1. Changing ε_0 from 4 to 8 deg in Eq. (6) has this effect.

Conclusions

1) V-tail panel geometric angles of attack and sideslip are functions of six variables: airplane angles of attack and sideslip, average downwash and sidewash angles, and V-tail dihedral and incidence.

2) In sample landing approach calculations sideslip angles of 17 deg, possibly reached in turbulence, are calculated to take left V-tail panels with 30 deg of dihedral to the stall point. The stall point is reached at a reduced sideslip angle of 14 deg for a dihedral angle of 40 deg.

3) In sideslip, induction from the opposite panel reduces local panel angles of attack, relative to the case for no sideslip. However, thicker boundary layers caused by crossflow would lead to lower panel stall angles, relative to the case without sideslip.

4) The critical sideslip angle for V-tail panel stall is reduced by 3 deg in the sample case, when the assumed sidewash is increased from 20 to 50% of the sideslip angle. The critical sideslip angle for V-tail stall is reduced to 12 deg when the downwash factor ε_0 is increased from 4 to 8.

References

[1]Purser, P. E., and Campbell, J. P., "Experimental Verification of a Simplified Vee-Tail Theory and Analysis of Available Data on Complete Models with Vee-Tails," NACA Rept. 823, 1945.

[2]McRuer, D. T., Ashkenas, I. L., and Graham, D., *Aircraft Dynamics and Automatic Control*, 1st ed., Princeton Univ. Press, Princeton, NJ, 1973, pp. 224–227.

[3]The Mathworks, Inc., *The Student Edition of MATLAB®, Version 5*, 1st ed., Prentice–Hall, Upper Saddle River, NJ, 1997, pp. 42–46.

Prediction of Laminar/Turbulent Transition in Airfoil Flows

Jeppe Johansen*
Risoe National Laboratory, 4000 Roskilde, Denmark
and
Jens N. Sørensen†
Technical University of Denmark, 2800 Lyngby, Denmark

Nomenclature

C_D = dissipation coefficient
C_f = skin-friction coefficient
G_γ = modeling constant
H = shape factor
H^* = kinetic energy shape parameter
Re_c = Reynolds number based on chord length
Re_x = Reynolds number based on distance from stagnation point
Re_θ = Reynolds number based on momentum thickness
$U_\tau = \sqrt{(\tau_w/\rho)}$ = friction velocity
u_e = velocity at the edge of the boundary layer
$x_{\rm tr}$ = transition point location
$y^+ = yU_\tau/\nu$ = nondimensional distance from wall
α_i = imaginary part of spatial wave number
γ = intermittency function
δ = boundary-layer thickness
δ_3 = kinetic energy thickness
δ^* = displacement thickness
θ = momentum thickness
ν = viscosity
ξ = streamwise coordinate
ϕ = amplitude of perturbation

Presented as Paper 98-0702 at the AIAA 36th Aerospace Sciences Meeting, Reno, NV, 12–15 January 1998; received 6 December 1998; revision received 10 March 1999; accepted for publication 20 March 1999.

*Ph.D. Student, Wind Energy and Atmospheric Physics Department, P.O. Box 49.

†Associate Professor, Department of Energy Engineering.

Introduction

COMPUTATION of flows over airfoils is a challenging problem because of the various complex phenomena connected with the occurrence of separation bubbles and the onset of turbulence. In many engineering applications involving weak streamwise pressure gradients and small curvature effects, turbulent quantities can be predicted well assuming fully turbulent flow. In the case of low-Reynolds-number airfoil flows [$Re < o(10^6)$], proper modeling of the transition point is crucial for predicting leading-edge separation. The transition prediction algorithm must be reliable because the transition point may affect the termination of a transitional separation bubble and hence determine bubble size and associated losses. This again has a strong influence on airfoil characteristics, with drag being the most affected.

A popular transition prediction model is the empirical criterion by Michel.[1] As shown in Refs. 2 and 3, this model gives fairly good results for many airfoil flows. In the present study the more general e^n method, proposed originally by Smith[4] and van Ingen,[5] is compared to the Michel criterion. The e^n method is based on linear stability analysis using the Orr–Sommerfeld equation to determine the growth of spatially developing waves. There have been several attempts by Drela and Giles[6] and Cebeci[7] to apply simplified versions of the e^n method in combination with the viscous-inviscid interaction algorithm.

In the present work a database on stability, with integral boundary-layer parameters as input, has been established. This database avoids the need for computing growth rates for each velocity profile. Furthermore, in order not to determine boundary-layer parameters such as displacement thickness, momentum thickness, and boundary-layer edge velocity using a Navier–Stokes (NS) solver, the NS solver is combined with an integral boundary-layer formulation.

Methods

Flow Solver

The results determined in the present study are computed using EllipSys2D, a general purpose two-dimensional incompressible NS solver, developed by Michelsen[8,9] and Sørensen[10] and based on a multiblock finite volume discretization of the Reynolds averaged NS equations in general curvilinear coordinates. The code uses primitive variables (u, v, and p). The pressure-velocity coupling is obtained with the SIMPLE method by Patankar[11] for steady-state calculations. Solution of the momentum equations is obtained using a second-order upwind scheme. The steady-state calculations are accelerated by the use of local time stepping and a three-level grid sequence.

The turbulence model employed in the present work is the two-equation k–ω SST (shear stress transport) turbulence model by Menter,[12] who obtained good predictions in flows with adverse pressure gradients.

Transition Prediction Models

In the present study two different transition prediction models are used. These are the empirical one-step model of Michel[1] and a semi-empirical e^n model based on linear stability in the form of a database, as suggested by Stock and Degenhart.[13] The Michel criterion is a simple model based on experimental data that correlates local values of momentum thickness with position of the transition point. It simply states that transition takes place where

$$Re_{\theta,\rm tr} = 2.9 Re_{x,\rm tr}^{0.4} \tag{1}$$

The second model is based on linear stability theory and is referred to as the e^n model by Smith[4] and van Ingen.[5] Linear stability